Korean J. Chem. Eng., 37(7), 1157-1165 (2020)
DOI: 10.1007/s11814-020-0516-3

pISSN: 0256-1115
eISSN: 1975-7220

Fabrication of magnetic cobalt ferrite nanocomposites: an advanced method of removal of toxic dichromate ions from electroplating wastewater

Bharti Verma† and Chandrajit Balomajumder

Department of Chemical Engineering, IIT Roorkee, Roorkee, India 24766
(*Received 18 November 2019 • Revised 24 January 2020 • Accepted 17 February 2020*)

Abstract−Magnetic cobalt ferrites ($CoFe_2O_4$) were synthesized by sol-gel method. These nanoparticles were ultra-sonicated with surface modified multi-walled carbon nanotubes (SM-MWCNTs) to form $CoFe_2O_4$/SM-MWCNTs nanocomposites. The as-prepared materials were used as an adsorbent for the removal of hexavalent chromium (Cr(VI)) arising from the presence of dichromate ions ($Cr_2O_7^{2-}$) in the electroplating effluent. The synthesized nanocomposites were characterized by field emission scanning electron microscopy (FESEM), transmission electron microscopy (TEM), X-Ray diffraction (XRD), Fourier transmission infrared spectroscopy (FT-IR), raman spectroscopy, thermo-gravimetric analysis (TGA), and zeta analyzer. The effect of the environmental chemistry of the solution on the adsorption has been discussed. The adsorption isotherm of Cr(VI) adsorption onto the as-synthesized $CoFe_2O_4$/SM-MWCNTs best fitted the Langmuir Adsorption Isotherm model. The high adsorption capacity of 100 mg/g was achieved at 40 °C under optimized conditions. Besides, the magnetic properties of synthesized $CoFe_2O_4$/SM-MWCNTs nanocomposites allow them to separate from the aqueous solution by magnetization easily. Even after seven consecutive adsorption-desorption cycles, the $CoFe_2O_4$/SM-MWCNTs nanocomposites presented an efficiency loss of less than 20% for the removal of Cr(VI) ions. This study clearly shows that cobalt nanocomposites are promising candidates in environmental applications.

Keywords: Cobalt Ferrites, Nanocomposites, Nanotubes, Heavy Metal, Electroplating

INTRODUCTION

Nanotechnology is the cutting-edge technology of materials science and engineering, which is gaining researchers' interest worldwide due to their varied applications. It is being explored for energy as well as environmental applications [1]. Carbon nanomaterials, especially carbon nanotubes (CNTs) with their exciting optical, electronic, mechanical, thermal, and chemical properties, have remained at the forefront of nanotechnology [2]. Owing to their vast surface area as well as large pore volumes, they have been utilized in treating heavy metal contaminated wastewater. The adsorption performance of CNTs is much better than conventional adsorbents such as activated carbon, silica, zeolites, chitosan, and polymers. This is attributable to their high surface area, tunable surface chemistry, non-corrosive chemistry, scalable production, and the presence of surface oxygen-containing functional groups. Despite their excellent characteristics, however, pure nanomaterials are limited for many applications. Therefore, the functionalization of CNTs, synthesis of carbon-based nanocomposites and nanohybrids are gaining researchers' interest worldwide [3]. These hybrids are much more durable and have more controlled functionalities when compared to pure nanomaterials. The magnetic modification of these CNTs by using metal ferrite nanoparticles is a novel way of making them suitable in magnetic data storage, drug delivery, and even more efficient environmental applications [4].

The development of these two materials (CNTs and metal ferrite nanoparticles) results in extremely strong nanocomposites having exciting properties, making them suitable for a varied range of applications [5]. The easier recovery of magnetic nanoparticles and the high surface area of CNTs lead to the development of new sorbents.

The present work focusses on the doping of cobalt ferrites ($CoFe_2O_4$) onto surface modified multi-walled carbon nanotubes (SM-MWCNTs) to form novel $CoFe_2O_4$/SM-MWCNTs nanocomposites and their application in the treatment of electroplating effluent. Cobalt ferrite ($CoFe_2O_4$) nanoparticles were chosen due to their high saturation magnetization and high coercivity [6]. Therefore, $CoFe_2O_4$ nanoparticles were synthesized by the sol-gel technique. These nanoparticles were then decorated over multi-walled carbon nanotubes (MWCNTs) to form $CoFe_2O_4$/SM-MWCNTs nanocomposites. These nanocomposites were then investigated for their adsorptive capacity for the removal of hexavalent chromium from electroplating effluent. The optimization of parameters was attained and various kinetic, thermodynamic, and isotherm studies were performed.

EXPERIMENTAL SECTION

1. Materials

All the reagents used were of analytical grade and were used as such. All the chemicals, including cobalt nitrate hexahydrate [$Co(NO_3)_2 \cdot 6H_2O$], ferric nitrate nonahydrate [$Fe(NO_3)_3 \cdot 9H_2O$], citric acid [$C_6H_8O_7$], potassium dichromate ($K_2Cr_2O_7$) were purchased from Sigma-Aldrich Chemical Reagent Co. All the solutions were made

†To whom correspondence should be addressed.
E-mail: bverma@ch.iitr.ac.in
Copyright by The Korean Institute of Chemical Engineers.

with double distilled water. The electroplating effluent was collected from Bharat Electronica Limited (B.E.L), Kotdwar, Uttarakhand, India.

2. Nanoparticle Preparation

The cobalt ferrite ($CoFe_2O_4$) nanoparticles were prepared by the sol-gel auto-combustion method. Cobalt nitrate, iron nitrate nonahydrate, and citric acid with a specific molar ratio were dissolved in milli-Q water. The reaction mixture was heated at 60 °C until sol formation. The temperature was suddenly increased to 80 °C on the onset of sol formation. The sol on heat treatment became viscous, and a gel-type material was obtained. The gel began frothing after the evaporation of total moisture. The gel automatically ignited after keeping in an oven at 200 °C for 2 hours. Colored ashes of $CoFe_2O_4$ nanoparticles were obtained after the completion of auto-ignition. $CoFe_2O_4$ nanoparticles were obtained after calcination at 500 °C.

3. Surface Modified Multi-walled Carbon Nanotubes (SM-MWCNTs)

The MWCNTs were acquired from Platonic Nanotech Private Ltd. These MWCNTs had a purity higher than 97%, an external diameter between 10-20 nm, and an approximate length between 10 and 30 μm. The surface of MWCNTs was modified by using 150 mL of HNO_3 (69%) solution. The mixture of a specific amount of MWCNTs and HNO_3 solution was agitated on a magnetic stirrer for 5 hours at a temperature of 80 °C. Repetitive vacuum filtration was done till the solution became neutral and all traces of HNO_3 from the sample were removed. After that, the sample was subjected to drying in a hot air oven at 80 °C for 4 hours.

4. Magnetic $CoFe_2O_4$/SM-MWCNTs Nanocomposite

The surface treatment of MWCNTs with acid was done to increase the hydrophilicity of the carbon nanotubes. The introduction of functional groups like -COOH, -CO, -OH on the surface of MWCNTs acts as active sites for the attachment of metal ferrites [7]. The sonication helps to vigorously agitate the solution and for uniform dispersion of metal ferrites onto the SM-MWCNTs. Therefore, $CoFe_2O_4$/SM-MWCNTs nanocomposites were obtained ultrasonically. $CoFe_2O_4$ nanoparticles and the SM-MWCNTs were added in ethanol in a specific ratio. This mixture was sonicated for about 60 minutes, then centrifuged at 8,000 rpm for 11 minutes at a low temperature. The nanocomposites were obtained after drying the solid product under vacuum.

5. Batch Adsorption Experiments

The adsorption experiments were performed as a function of solution initial pH (2-14), adsorbent dose (0.05-0.15 gm), temperature (20 °C to 40 °C), contact time (2-24 hr), initial Cr(VI) concentration (100-200 mg/L). The experiments were carried out on a rotary shaker with 125 mL conical flasks. About 50 mL of different concentrations of Cr(VI) solutions were shaken for different periods of time. The adsorption capacity was calculated as

$$q_e = \frac{(C_0 - C_e)V}{m} \quad (1)$$

where C_0 (mg/L) is the initial concentration of Cr(VI) ion; C_e (mg/L) is the concentration of Cr(VI) ion after an elapsed absorption time t; q_e (mg/g) is the sorption capacity, m (g) is the adsorbent mass used, and V (L) is the solution volume [8]. After the attainment of equilibrium, the sample solutions were filtered and collected for analysis.

6. Experimental Characterization

All the experimental characterizations were performed in the Institute Instrumentation Centre, Indian Institute of Technology, Roorkee, India. The electroplating effluent was analyzed for its heavy metal composition by inductively coupled plasma mass spectroscopy (ICP-MS-Perkin Elmer-ELAN DRC-e) and ion chromatography. The surface morphology of the materials was characterized by FESEM (Carl Zeiss Ultra Plus Model). The micromorphology was obtained by TEM (FEI Tecnai G2 20 S-Twin). The crystal structure was determined by XRD analysis by a Bruker D8 advance at an angle range of 5°-90°. The FTIR spectra were obtained using a Perkin-Elmer BX series FT-IR-5000 spectrophotometer (Perkin Elmer, Nicolet, USA). The thermal analysis of the materials was done by thermo gravimetric/differential thermal analyzer (TG/DTA)

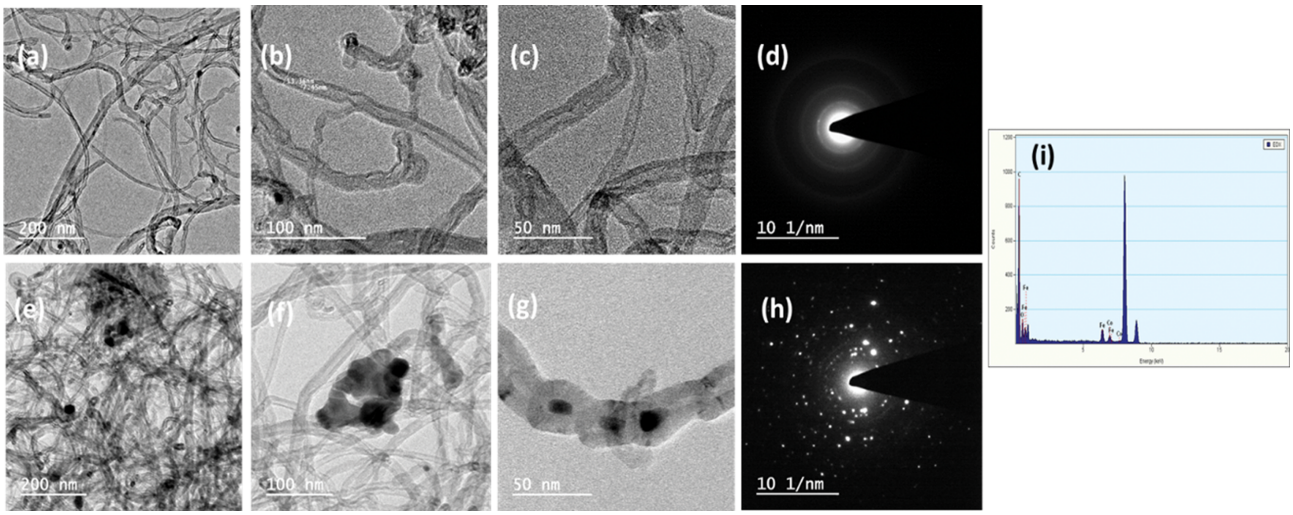


Fig. 1. TEM images of (a)-(d) MWCNTs at 200 nm, 100 nm, 50 and 10 1/nm, (e)-(h) $CoFe_2O_4$/SM-MWCNTs at 200 nm, 100 nm, 50 and 10 1/nm and (i) EDAX of $CoFe_2O_4$/SM-MWCNTs.

(Model-SII 6300 EXSTAR) in a nitrogen atmosphere at a flow rate of 200 ml/min. The temperature range was kept between room temperature and 1,200 °C. The zeta potential was measured in a aeta potential and nano size particle analyzer" in the Chemical Engineering department at IIT Roorkee. The filtrates after the adsorption were analyzed for their chromium concentration using a standard diphenyl carbazide method using a UV visible spectrophotometer (HACH DR5000) [9].

7. Quality Assurance

To corroborate the reliability of the analytical data, sufficient quality control measures were taken. Therefore, all the experiments were conducted three times to ensure that the analytical results were reproducible. The average data has been shown here. It was found that the data was reproducible, and the error was within ±2%. To confirm the removal of Cr(VI) was due to adsorption, a blank experiment was run to prove that the Cr(VI) concentration did not change with time.

RESULTS AND DISCUSSION

1. Morphology of the Materials

TEM was used at various magnifications to explore the morphology of the materials. Fig. 1(a) demonstrates that MWCNTs are tubular structures with an average outer diameter of around 15 to 20 nm, which was in accordance with the specifications given by the manufacturer. Fig. 1(d) shows diffused rings that indicate that

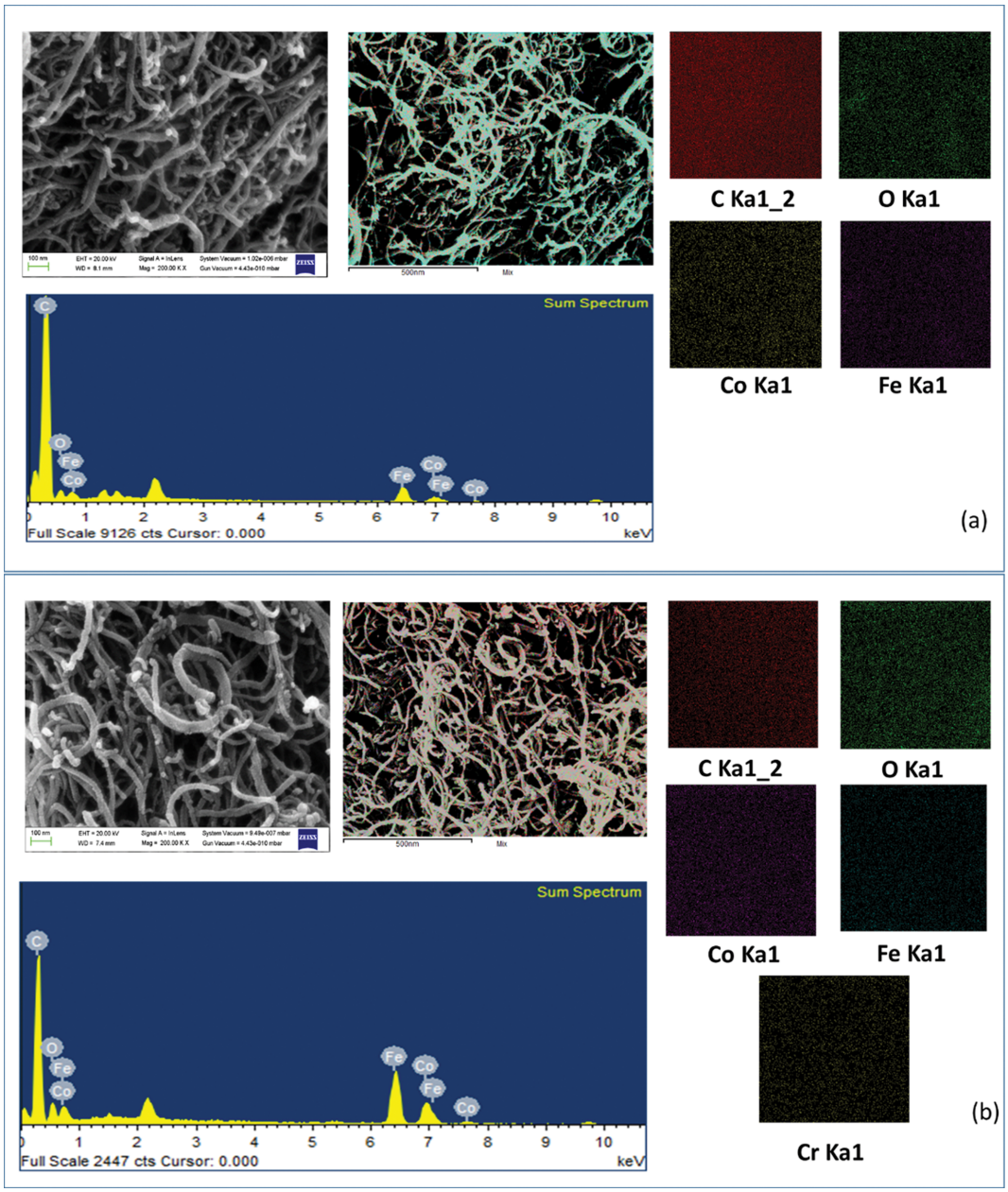


Fig. 2. FESEM images of $CoFe_2O_4$/SM-MWCNTs (a) before and (b) after Cr(VI) adsorption.

the MWCNTs are amorphous. The TEM images of $CoFe_2O_4$/SM-MWCNTs clearly demonstrate the embedded cobalt ferrite nanoparticles onto the surface of MWCNTs. The presence of cobalt and iron is confirmed by the EDAX analysis presented in Fig. 1(i).

The FESEM images of $CoFe_2O_4$/SM-MWCNTs nanocomposites before and after adsorption of Cr(VI) are shown in Fig. 2. It can be observed that the tubular $CoFe_2O_4$/SM-MWCNTs nanocomposites are present in the tangled form. The average outer diameter is 30-40 nm as shown. Since the purchased MWCNTs have an average outer diameter of 10-20 nm, it depicts that there is a layer of magnetic cobalt ferrite nanoparticles embedded onto the surface of SM-MWCNTs. Fig. 2(b) clearly shows that the average outer diameter has increased to about 35-60 nm, which is indicative of Cr(VI) adsorption onto the nanocomposites. The EDX analysis confirms the presence of components of $CoFe_2O_4$/SM-MWCNTs nanocomposites. Fig. 2(a) confirms the presence of cobalt and iron in the nanocomposites. Besides, Cr(VI) removal by these nanocomposites is proved by the additional presence of Chromium in Fig. 2(b).

2. Crystal Structure and FT-IR Spectroscopy

The crystal structure of MWCNTs synthesized $CoFe_2O_4$/SM-MWCNTs nanocomposites before and after the removal of Cr(VI) was determined by XRD as shown in Fig. 3(a). The MWCNTs demonstrate the typical diffraction peaks at 2θ=25.89° and 42.47°, corresponding to the (002) and (100) planes of graphite (JCPDS no. 00-002-0456). The d-spacing value of 3.41 Å of (002) plane is representative of the distance between the graphite sheets [10]. The XRD analysis of $CoFe_2O_4$/SM-MWCNTs depicts that the peak at 25.89° has become weak. This indicates a decrease in crystallinity due to the interaction between MWCNTs and cobalt ferrites. The XRD pattern of $CoFe_2O_4$/SM-MWCNTs nanocomposites matches well with the cubic phase of iron that the diffraction peaks (2θ= 44.67° and 65.02°) correspond to the (110) and (200) planes of ferrites, respectively. The intense peak at 35.44° with the d-spacing value of 2.53 Å is a characteristic peak of magnetite [10]. The peaks at (2θ=18.29°, 30.085°, 35.44°, 37.058°, 43.059°, 56.97°, 62.53°) correspond to (003), (104), (113), (006), (024), (125) and (208) planes of rhombohedral crystal of cobalt iron oxide ($CoFe_2O_4$) (JCPDS no. 01-079-1744) [11]. The new peaks observable in the XRD pattern of $CoFe_2O_4$/SM-MWCNTs after Cr(VI) adsorption at 37.32°, 43.36°, and 74.55° correspond to planes (222), (400) and (533) of cubic crystal of iron cobalt-chromium oxide (JCPDS no. 01-076-2496). This confirms the interaction of Cr(VI) with the nanocomposites.

FT-IR spectroscopy is often used to determine the surface functional groups of the materials. The peaks as seen in Fig. 3(b) at 3,440 cm^{-1} and 1,072 cm^{-1} are attributed to O-H stretching vibrations [12]. This is because the oxidation of MWCNTs before the addition of cobalt ferrites produces hydroxyl groups on the surface of MWCNTs. The hydrophilicity of the MWCNTs is thereby increased. The band at 1,200-1,240 cm^{-1} and the peak at 1,650 cm^{-1} demonstrate the presence of the carboxyl group (-COOH). The peak at 2,920 cm^{-1} is attributed to -CH_2 stretching vibrations. The FT-IR spectra of synthesized nanocomposites show that the intensity of the peaks of the carboxyl group, hydroxyl group has weakened. This is due to the interaction of cobalt ferrites with the MWCNTs. The sharp peak at 576 cm^{-1} in the FT-IR spectra of $CoFe_2O_4$/SM-MWCNTs nanocomposites is attributed to Fe (Co)-O band [13].

3. Raman Spectroscopy and Thermo-gravimetric Analysis

Raman spectroscopy was performed to determine the interaction amongst the components in the formation of $CoFe_2O_4$/SM-

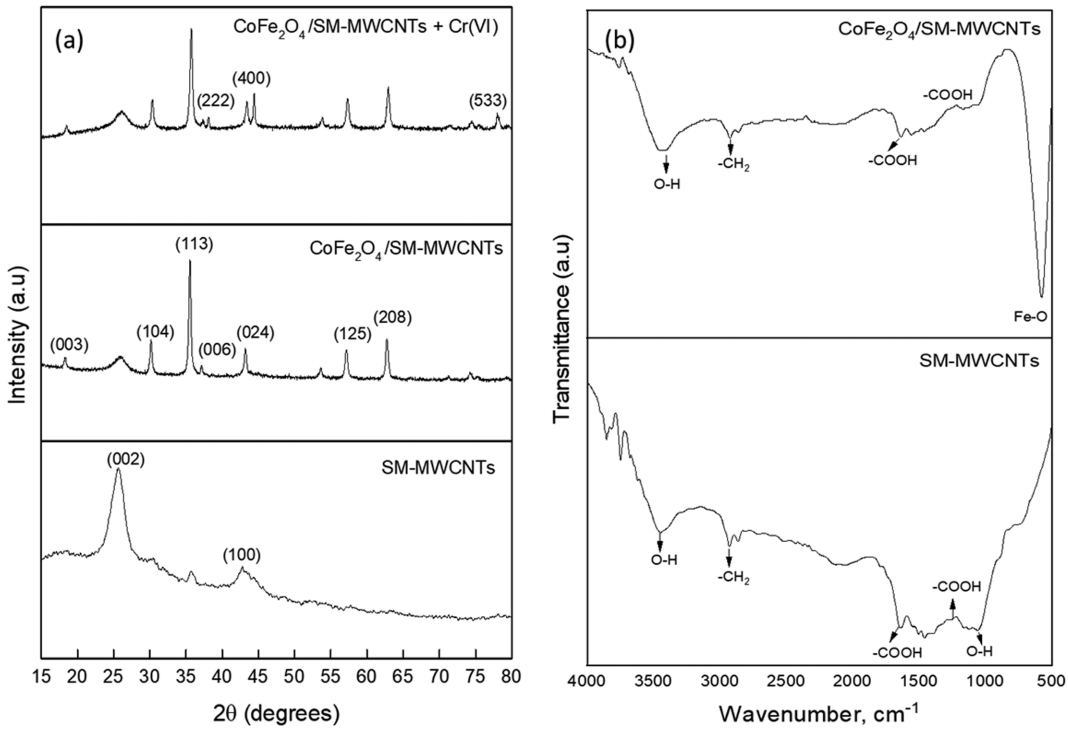


Fig. 3. (a) XRD (b) FTIR spectra of the materials.

MWCNTs nanocomposites. The Raman spectra of MWCNTs show a peak at 1,344 cm^{-1} which demonstrates the D-band of the C-C bond, referring to graphitic structure disorders. The peak at 1,574 cm^{-1} exhibits the G-band indicative of the C=C carbon sp^2 bond. The D/G ratio was calculated to be 0.92 for MWCNTs. The D and G bands of the oxidized MWCNTs are displaced to 1,346 cm^{-1} and 1,570 cm^{-1}, respectively. The D/G ratio of the oxidized MWCNTs was evaluated to be 1.42. In the spectra of synthesized $CoFe_2O_4$/SM-MWCNTs, the bands are displaced to 1,349 cm^{-1} and 1,577 cm^{-1}, respectively. The D/G ratio of the nanocomposites was evaluated to be 1.59. The increase in the D/G ratio occurring due to the interaction of $CoFe_2O_4$ nanoparticles and MWCNTs is a clear indication of more significant distortions in its crystal structure [14]. The results demonstrate strong interactions between cobalt ferrites and MWCNTs.

TGA quantifies the molar mass of the functional groups that are present on the surface of the materials. The TGA profile of oxidized MWCNTs exhibits two main weight loss regions. The first weight loss region (approximately 3.34%) can be attributed to the loss of external water molecules as well as the carboxyl group added during acid treatment of MWCNTs. The weight loss of 91.02% was observed when the temperature became 1,079 °C. This might be attributed to the gasification of MWCNTs at which its decomposition begins. There was no weight loss after 1,079 °C. It can be inferred that the thermal stability of raw MWCNTs is quite high. The TGA profile of the $CoFe_2O_4$/SM-MWCNTs shows the same trend as MWCNTs. The initial 3.6% weight loss to 500 °C can be attributed to the external water molecules and the carboxyl groups. A 54% weight loss was observed when the temperature was increased from 514.08 °C to 710 °C. The profile of $CoFe_2O_4$/SM-MWCNTs after Cr(VI) adsorption demonstrates an additional 1% loss at 450 °C, which can be attributed to the attached heavy metal ion. Besides, there is a weight loss of 49% when the temperature is increased from 437.09 °C to 660.84 °C. The DTG profiles of these materials are shown in Fig. 4(c). The raw MWCNTs show an endothermic peak in the temperature range of 704 °C to 1,067 °C. The $CoFe_2O_4$/SM-MWCNTs show strong adsorption peaks at 661 °C and 586 °C before and after Cr(VI) adsorption, respectively.

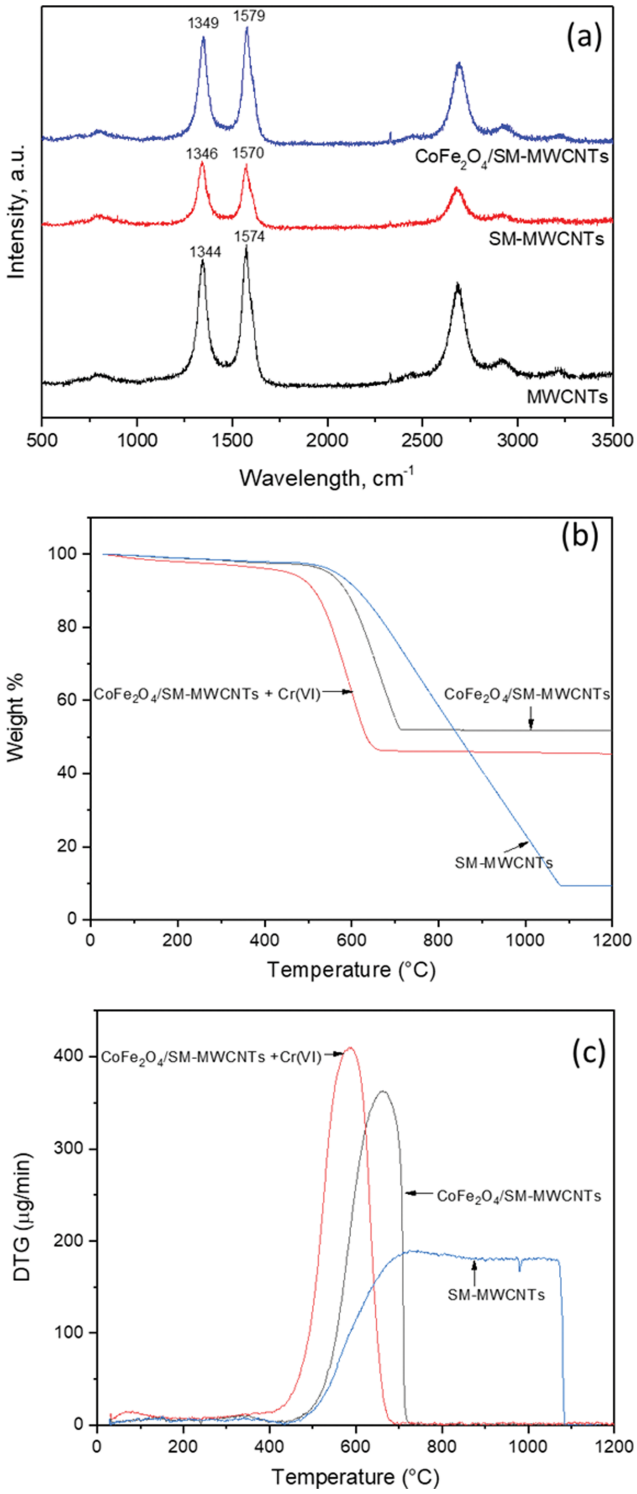


Fig. 4. (a) Raman spectroscopy (b) TGA (c) DTG of the materials.

4. Effect of Initial pH of Solution on Cr(VI) Adsorption by $CoFe_2O_4$/SM-MWCNTs

The solution pH is a crucial factor in the process of adsorption. The structure at the surface of the material and the concentration of hydrogen ions are dependent on the pH of the solution. Fig. 5 shows the maximum removal of Cr(VI) by $CoFe_2O_4$/SM-MWCNTs nanocomposites is obtained at a low pH. The high adsorption at a lower pH may be attributed to the species of Cr(VI) present in the solution. At lower pH, the Cr(VI) is mainly present in its monovalent form of $HCrO_4^-$. At the same concentration, the adsorption free energy of $HCrO_4^-$ is smaller than that of other species of Cr(VI) such as CrO_4^{2-} and $Cr_2O_7^{2-}$ [15]. Also, the presence of hydronium ions at low pH makes the surface of adsorbent positive, thereby attracting the anionic Cr(VI) species.

MWCNTs have a zero-point charge (ZPC) of 5.1 [16]. The ZPC of the as-produced $CoFe_2O_4$/SM-MWCNTs is 6.88. Therefore, if the solution of pH is less than 6.88, the surface of the nanocomposite is protonated. This helps in the removal of negatively charged Cr(VI) species due to electrostatic attraction. Beyond the pH_{PZC}, the surface of the composite becomes negative, and hence the removal of anions is reduced. The highest removal (88% in 1 hour) of Cr(VI) is observed at a pH of 2 with a slight decline till pH 6. However, an interesting observation was made. The percent decline in efficiency beyond pH_{PZC} was not massive. The percent removal

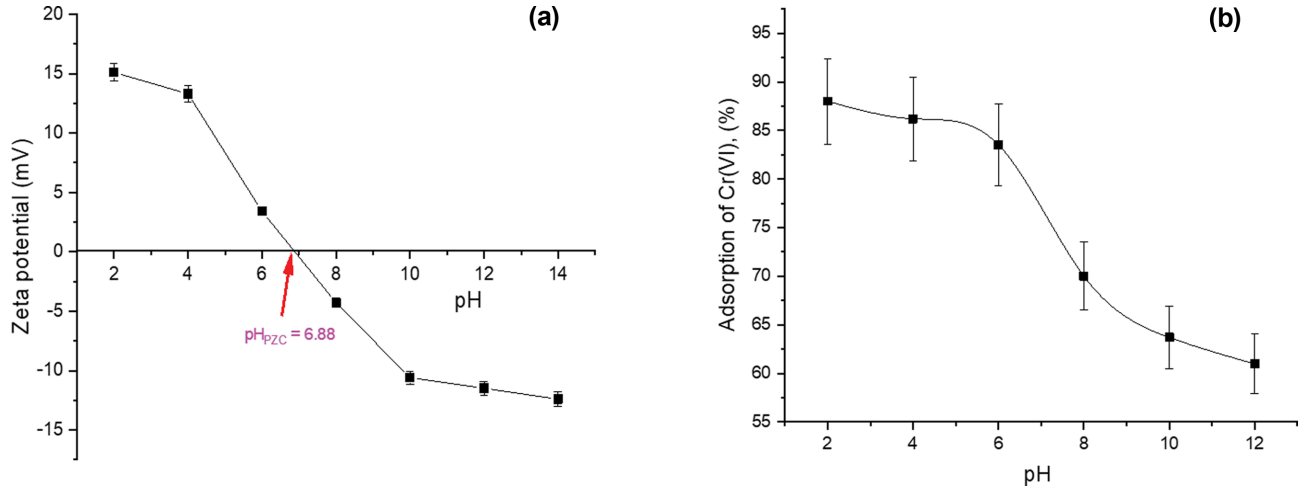


Fig. 5. (a) Zeta potential of $CoFe_2O_4$/SM-MWCNTs (b) effect of pH on Cr(VI) adsorption.

of Cr(VI) by nanocomposites was 88% and 61% at pH values of 2 and 12, respectively. This was because a complex is formed between Cr(VI) and ferric ion of Iron oxide as per the following equation [17].

$$-(FeOH)_2 + CrO_4^{2-} \xrightarrow{yields} -(Fe)_2 - CrO_4 + 2OH^- \quad (2)$$

Besides, iron oxide has more affinity towards $Cr_2O_4^-$ than OH^-, thereby the removal of Cr(VI) by $CoFe_2O_4$/SM-MWCNTs is achieved by ion exchange [18].

5. Kinetics of Adsorption

The batch adsorption experiments were carried under optimum conditions and were run for a long time. About 50 mL of 100 mg/L Cr(VI) solutions was shaken with 0.1 g $CoFe_2O_4$/SM-MWCNTs at 40 °C. The optimum pH of 2 was maintained by using 0.1 M H_2SO_4. It is observed that the adsorption equilibrium was reached within 180 minutes for Cr(VI). The Cr(VI) demonstrates high-speed kinetics, obtaining 88% removal in the first 60 minutes. This rapid adsorption is attributed to the available number of sites at the beginning, which reduces with time [19].

The adsorption of Cr(VI) was evaluated using pseudo-first-order, pseudo-second-order, and intra-particle diffusion models. The linearized models are shown in Table 1.

The pseudo-second-order model exhibited a good fit, with a correlation coefficient of 0.994 as seen in Table 2. Therefore, the adsorption of Cr(VI) by $CoFe_2O_4$/SM-MWCNTs is limited by chemical adsorption. To determine whether the adsorption kinetics is controlled by boundary layer diffusion or intra-particle diffusion, or both, the Weber Morris model (Intra-particle diffusion model) was applied. If the intercept is zero, the adsorption is predominantly controlled by the intra-particle diffusion model. Whereas, if the plot gives more than one straight line, both boundary layer and intra-particle diffusion are controlling the adsorption mechanism. The intra-particle diffusion plot presents two regions for the Cr(VI) adsorption kinetic data. Therefore, both boundary layer diffusion and intra-particle diffusion play a crucial role in the adsorption of Cr(VI) onto the nanocomposites.

Table 1. Kinetic models

Kinetics model	Equation	References
Pseudo-first-order	$\log_e(q_e - q) = \log_e q_e - K_1 t$	[20]
Pseudo-second-order	$\frac{t}{q_t} = \frac{1}{K_2 q_e^2} + \frac{1}{q_e} t$	[21]
Weber morris model (intra-particle diffusion)	$q_t = K\sqrt{t} + C$	[8]

6. Adsorption Isotherms and Thermodynamics

The batch adsorption experiments were conducted at temperatures of 25, 30, 35, and 40 °C and were then applied to the Langmuir and Freundlich isotherm model. About 50 mL of Cr(VI) solutions of different concentrations ranging from 100 mg/L to 200 mg/L were shaken with 0.1 g $CoFe_2O_4$/SM-MWCNTs. The optimum pH of 2 was maintained by using 0.1 M H_2SO_4.

6-1. Langmuir Adsorption Isotherm Model

The Langmuir equation [22] can be written as:

$$q_e = \frac{q_m b C_e}{1 + b C_e} \quad (3)$$

The linearized form of the above equation is:

$$\frac{C_e}{q_e} = \frac{1}{q_m b} + \frac{1}{q_m} C_e \quad (4)$$

Table 2. Kinetic parameters

Pseudo first order model			Pseudo second order model			Intra-particle diffusion model	
q_e mg·g^{-1}	K_1	R^2	q_e	K_1	R^2	K_{ip} (g mg^{-1} hr$^{-1/2}$)	R^2
32.20	0.022	0.93	55.56	0.046	0.994	15.13	0.7

Table 3. Isotherm constants at different temperatures

Isotherm constants for the Cr(VI) adsorption onto $CoFe_2O_4$/SM-MWCNTs at different temperatures							
Temperature (°C)	Langmuir model				Freundlich model		
	q_{max} (mg·g^{-1})	b (L·mg^{-1})	R_L (L·mg^{-1})	R^2	K_f (mg·g^{-1})	n	R^2
25	96.15	2.81	0.0035	0.996	6.23	6.58	0.97
30	97.087	4.90	0.0020	0.995	6.46	6.73	0.97
35	98.04	7.85	0.0013	0.994	6.69	10.41	0.95
40	100	11.11	0.00089	0.992	6.82	11.40	0.92

where, q_e (mg/g) is the sorption capacity at equilibrium; C_e (mg/L) is the adsorbate concentration at equilibrium; q_m is the maximum sorption capacity, and b is the Langmuir constant which is associated with the energy of adsorption [23]. By plotting a graph between C_e/q_e Vs C_e, q_m and b can be determined. Also, the adsorption isotherms can be analyzed in terms of the separation factor, R_L, which is defined as:

$$R_L = \frac{1}{1+bC_0} \quad (5)$$

If R_L value lies between 0 and 1, the adsorption is favorable, whereas it is not the case for all other values [24].

6-2. Freundlich Adsorption Isotherm Model

The Freundlich adsorption isotherm equation [25] can be represented as:

$$q_e = K_f C_e^{1/n} \quad (6)$$

The linearized form of the above equation can be conveniently represented as:

$$\log q_e = \log K_f + \frac{1}{n}\log C_e \quad (7)$$

where K_f and n are the constants of the Freundlich isotherm model. The value of n lying between 1 to 10 is an indication of favorable adsorption [25].

As seen from Table 3, the $CoFe_2O_4$/SM-MWCNTs has a high Cr(VI) adsorption capacity of 96.15 mg/g at room temperature and a pH of 2. The Cr(VI) adsorption capacity rose to 100 mg/g when the temperature was increased to 40 °C. This increase of adsorption capacity with temperature is indicative of an endothermic reaction. The R_L value shows that the adsorption is favorable.

The adsorption follows the pseudo-second-order kinetics and Langmuir isotherm model. These results suggest that the adsorption of Cr(VI) by $CoFe_2O_4$/SM-MWCNTs is limited by chemical adsorption. The FTIR spectra of $CoFe_2O_4$/SM-MWCNTs confirm the presence of oxygen-containing groups. It can be safely said that the predominant mechanism involved is the ion-exchange mechanism since there is a huge possibility of ion exchange between the heavy metal and the protons on the oxygen-containing functional groups [26]. The large surface area and large pore volumes of the MWCNTs are contributing to the obtained high adsorption capacity.

One of the arguments favoring the high adsorption capacity of Cr(VI) by $CoFe_2O_4$/SM-MWCNTS at a low pH could be the reduction of Cr(VI) to Cr(III). Some of the Cr(VI) is reduced to Cr(III), especially at low pH. The reduction reactions are as follows [27]:

$$HCrO_4^- + 7H^+ + 3e^- \leftrightarrow Cr^{3+} + 4H_2O \quad (8)$$

$$Cr_2O_7^{2-} + 6e^- + 3H^+ \leftrightarrow 2Cr^{3+} + 7H_2O \quad (9)$$

7. Reusability of $CoFe_2O_4$/SM-MWCNTs Nanocomposites

It is imperative to determine the reusability of the adsorbent for practical applications. The $CoFe_2O_4$/SM-MWCNTs showed that it remains quite efficient after many adsorption-desorption cycles as can be seen from Fig. 6(a). An efficiency loss of less than 20% was observed even after seven consecutive adsorption-desorption cycles. Besides, the magnetic nature of the $CoFe_2O_4$/SM-MWCNTs allows

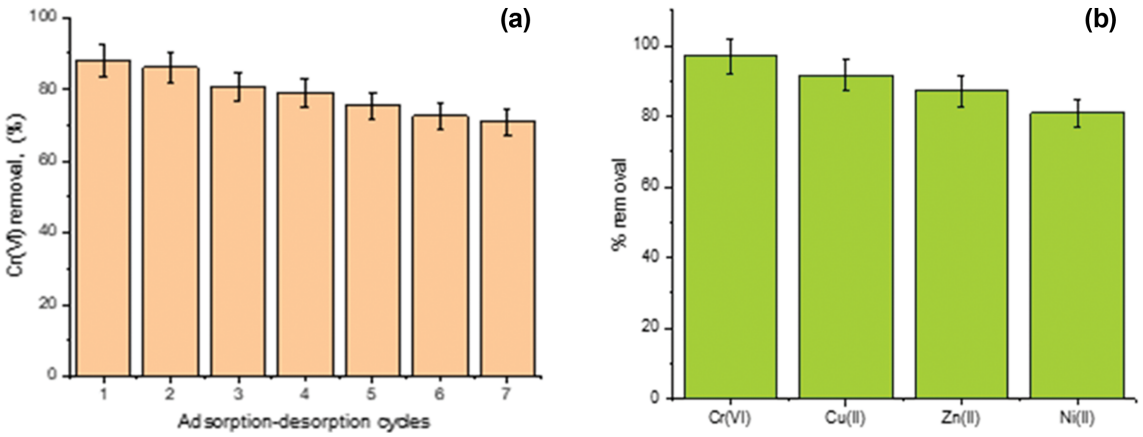


Fig. 6. (a) Desorption study (b) application to electroplating effluent.

Table 4. Characteristics of electroplating effluent

Parameter	Value
pH	2.2
Cr(VI)	178 ppm
Ni	16 ppm
Cu	25 ppm
Zn	20 ppm
Al	7 ppm
Na	110 ppm
Ca	100 ppm
Nitrate	10 ppm
As	1 ppm
Fluoride	10.2 ppm

for easy separation. The results suggest that the synthesized nanocomposites are efficient as well as durable.

8. Application of $CoFe_2O_4$/SM-MWCNTs in the Remediation of Electroplating Effluent

The optimum conditions of Cr(VI) removal by as-synthesized $CoFe_2O_4$/SM-MWCNTs was applied to the treatment of electroplating effluent as can be seen in Fig. 6(b). The characteristics of the electroplating effluent are presented in Table 4.

The as-synthesized $CoFe_2O_4$/SM-MWCNTs were efficient for adsorption of metals, where equilibrium removal percentages were 97% for Cr(VI), 91.6% for copper, 87.1% for zinc and 80.8% for nickel. The Cu(II), Zn(II) and Ni(II) ions are adsorbed by electrostatic attraction between these cations and the carboxyl/hydroxyl group present in the synthesized nanocomposites. The order of adsorption capacity of these metals is based on their pK values. The greater the pK value, the less is the adsorption affinity of metals. The highest pK value of 9.9 for nickel results in a decrease in the adsorption capacity [28]. The pK values for Cr(VI), Cu(II) and Zn(II) are 1.8, 7.9, and 9, respectively [10]. The comparison of the performance of as-synthesized materials with other adsorbents for Cr(VI) adsorption is shown in Table 5.

CONCLUSION

Magnetic cobalt ferrites were successfully prepared by the sol-gel technique. These nanoparticles were ultra-sonicated with oxidized MWCNTs to produce novel $CoFe_2O_4$/SM-MWCNTs nanocomposites. The as-synthesized $CoFe_2O_4$/SM-MWCNTs were tested for adsorption of Cr(VI) from electroplating effluent. The results indicate that at a pH of 2, 88% of Cr(VI) was removed within two hours of the experiment. Equilibrium was reached within 180 minutes, and 99.8% of Cr(VI) was removed. The experimental data were well fitted to the Langmuir isotherm model with a monolayer adsorption capacity of 100 mg/g at 40°. The adsorption was spontaneous, endothermic, and followed the pseudo-second-order model. The synthesized nanocomposites removed 97% Cr(VI), 91.6% Cu(II), 87.1% Zn(II) and 80.8% Ni(II) from the electroplating effluent sample. Even after seven consecutive reutilization cycles, an efficiency loss of less than 20% was observed. The structural integrity of these materials cannot be easily altered and they can be reused several times in the process. Therefore, the $CoFe_2O_4$/SM-MWCNTs can be utilized as a suitable and potential adsorbent in environmental pollution management due to their low cost and ease of synthesis.

Table 5. Adsorption capacities of various adsorbents for Cr(VI) removal

Adsorbents	Adsorption capacity (mg/g)	References
Silica nanotubes	42.9	[29]
Fibrillar magnetic carbon	43.17	[30]
Apple peels activated carbon	36.01	[31]
Magnetic magnetite nanoparticles	35	[32]
Modified carbon foam	33	[33]
Chitosan-based hydrogel	73.14	[34]
$CoFe_2O_4$/SM-MWCNTs	100	This study

SUPPORTING INFORMATION

Additional information as noted in the text. This information is available via the Internet at http://www.springer.com/chemistry/journal/11814.

REFERENCES

1. J. Xu, Z. Cao, Y. Zhang, Z. Yuan, Z. Lou, X. Xu and X. Wang, *Chemosphere*, **195**, 351 (2018).
2. S. Iijima, *Nature*, **354**, 56 (1991).
3. H. Chang and H. Wu, *Energy Environ. Sci.*, **6**(12), 3483 (2013).
4. R. Sepahvand and R. Mohamadzade, *J. Sci. Islam. Repub. Iran*, **22**(2), 177 (2011).
5. V. Georgakilas, D. Gournis, V. Tzitzios, L. Pasquato, M. Guldi and M. Prato, *J. Mater. Chem.*, **17**, 2679 (2007).
6. H. Zheng, J. Kreisel, Y. Chu, R. Ramesh and L. Salamanca-riba, *Appl. Phys. Lett.*, **90**, 113113 (2007).
7. T. N. Diva, K. Zare, F. Taleshi and M. Yousefi, *J. Nanostructure Chem.*, **7**, 273 (2017).
8. M. Hadi, M. Mohammad, A. Kumar and B. Heibati, *Chem. Eng. J.*, **279**, 344 (2015).
9. M. S. Gaikwad and C. Balomajumder, *J. Environ. Chem. Eng.*, **5**(1), 45 (2017).
10. J. O. M. Neto, C. R. Bellato and D. C. Silva, *Chemosphere*, **218**, 391 (2019).
11. W. Chen, Z. Lu, B. Xiao, P. Gu, W. Yao, J. Xing, A. M. Asiri, K. A. Alamry, X. Wang and S. Wang, *J. Clean. Prod.*, **211**, 1250 (2019).
12. P. A. M. Mourão, P. J. M. Carrott and M. M. L. Ribeiro Carrott, *Carbon*, **44**(12), 2422 (2006).
13. N. Li, M. Zheng, X. Chang, G. Ji, H. Lu, L. Xue, L. Pan and J. Cao, *J. Solid State Chem.*, **184**, 953 (2011).
14. T. Zhao, X. Ji, X. Guo, W. Jin, A. Dang, H. Li and T. Li, *Chem. Phys. Lett.*, **653**, 202 (2016).
15. C. Luo, Z. Tian, B. Yang, L. Zhang and S. Yan, *Chem. Eng. J.*, **234**, 266 (2013).
16. J. Hu, C. Chen, X. Zhu and X. Wang, *J. Hazard. Mater.*, **162**(2),

1542 (2009).
17. L. Tang, G. D. Yang, G. M. Zeng, Y. Cai, S. S. Li, Y. Y. Zhou, Y. Pang, Y. Y. Liu, Y. Zhang and B. Luna, *Chem. Eng. J.*, **239**, 114 (2014).
18. J. Hu, G. Chen and I. M. C. Lo, *Water Res.*, **39**(18), 4528 (2005).
19. M. H. Dehghani, M. M. Taher, A. K. Bajpai, B. Heibati, I. Tyagi, M. Asif, S. Agarwal and V. K. Gupta, *Chem. Eng. J.*, **279**, 344 (2015).
20. T. Wajima, Y. Umeta, S. Narita and K. Sugawara, *DES*, **249**(1), 323 (2009).
21. M. E. Argun, S. Dursun, C. Ozdemir and M. Karatas, *J. Hazard. Mater.*, **141**, 77 (2007).
22. Y.-H. Li, S. Wang, J. Wei, X. Zhang, C. Xu, Z. Luan, D. Wu and B. Wei, *Chem. Phys. Lett.*, **357**, 263 (2002).
23. A. Bhatnagar, E. Kumar and M. Sillanpää, *Chem. Eng. J.*, **163**(3), 317 (2010).
24. M. L. Paul, J. Samuel, S. B. Das, S. Swaroop, N. Chandrasekaran and A. Mukherjee, *Ind. Eng. Chem. Res.*, **51**, 46 (2012).
25. R. Milena, H. Buchtov and P. Jano, *Water Res.*, **37**, 4938 (2003).
26. X. Yang, Y. Wan, Y. Zheng, F. He, Z. Yu, J. Huang, H. Wang, Y. S. Ok, Y. Jiang and B. Gao, *Chem. Eng. J.*, **366**, 608 (2019).
27. S. Chen, Q. Yue, B. Gao and X. Xu, *J. Colloid Interface Sci.*, **349** (1), 256 (2010).
28. C. Cabrera, C. Gabaldón and P. Marzal, *J. Chem. Technol. Biotechnol.*, **80**(4), 477 (2005).
29. P. Wang, M. Du, H. Zhu, S. Bao, T. Yang and M. Zou, *J. Hazard. Mater.*, **286**, 533 (2015).
30. J. Huang, Y. Cao, Q. Shao, X. Peng and Z. Guo, *Ind. Eng. Chem. Res.*, **56**(38), 10689 (2017).
31. I. Enniya, L. Rghioui and A. Jourani, *Sustain. Chem. Pharm.*, **7**, 9 (2018).
32. S. Rajput, C. U. Pittman and D. Mohan, *J. Colloid Interface Sci.*, **468**, 334 (2016).
33. C. G. Lee, S. Lee, J. A. Park, C. Park, S. J. Lee, S. B. Kim, B. An, S. T. Yun, S. H. Lee and J. W. Choi, *Chemosphere*, **166**, 203 (2017).
34. P. B. Vilela, A. Dalalibera, E. C. Duminelli, V. A. Becegato and A. T. Paulino, *Environ. Sci. Pollut. Res.*, **26**(28), 28481 (2019).

Supporting Information

Fabrication of magnetic cobalt ferrite nanocomposites: an advanced method of removal of toxic dichromate ions from electroplating wastewater

Bharti Verma[†] and Chandrajit Balomajumder

Department of Chemical Engineering, IIT Roorkee, Roorkee, India 24766
(*Received 18 November 2019 • Revised 24 January 2020 • Accepted 17 February 2020*)

1. Magnetic Separation of $CoFe_2O_4$/SM-MWCNTs from the Solution

It was observed that after the $CoFe_2O_4$/SM-MWCNTs were added to the wastewater contaminated with Cr(VI), the color of the solution changed to black owing to the color of nanocomposites. The mixture was shaken properly for a definite period of time, and a permanent magnet was placed near the solution. The nanocomposites were attracted to the magnet because of their magnetic properties and the supernatant was almost colorless.

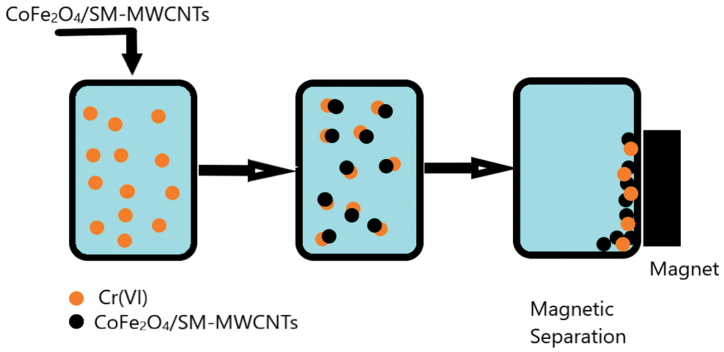


Fig. S1. Magnetic separation of $CoFe_2O_4$/SM-MWCNTs.

2. Kinetic of Adsorption

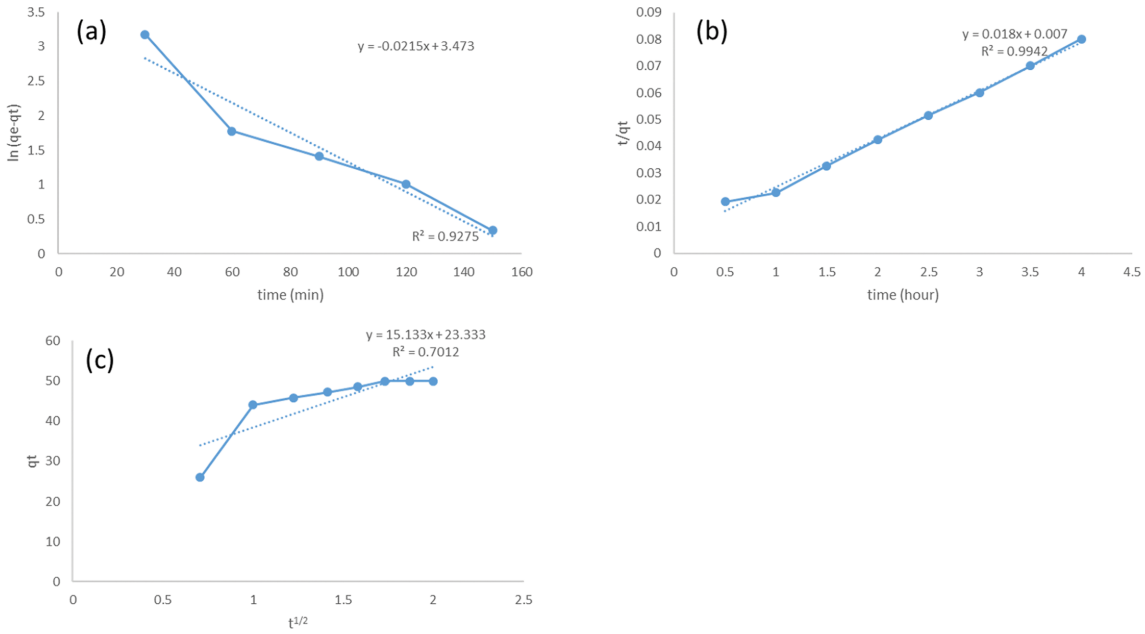


Fig. S2. (a) Pseudo first order (b) pseudo second order (c) intra particle diffusion.

3. Adsorption Isotherms

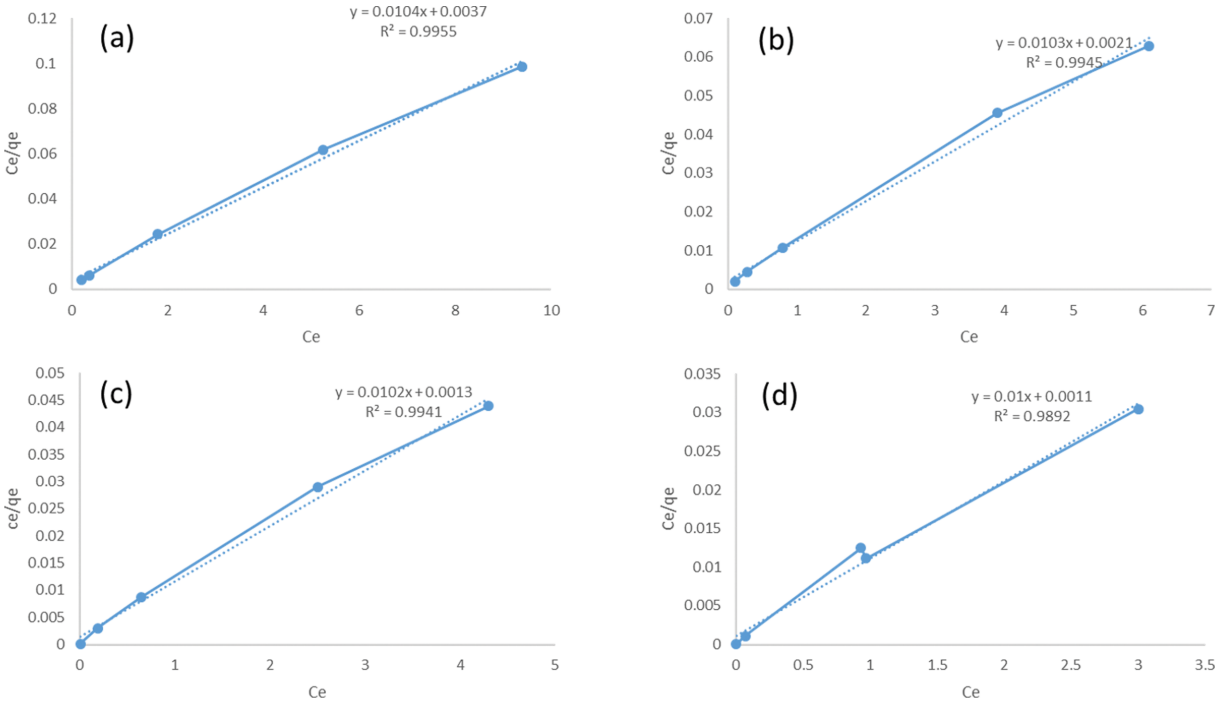


Fig. S3. Langmuir adsorption isotherm at (a) 25 °C (b) 30 °C (c) 35 °C and (d) 40 °C.

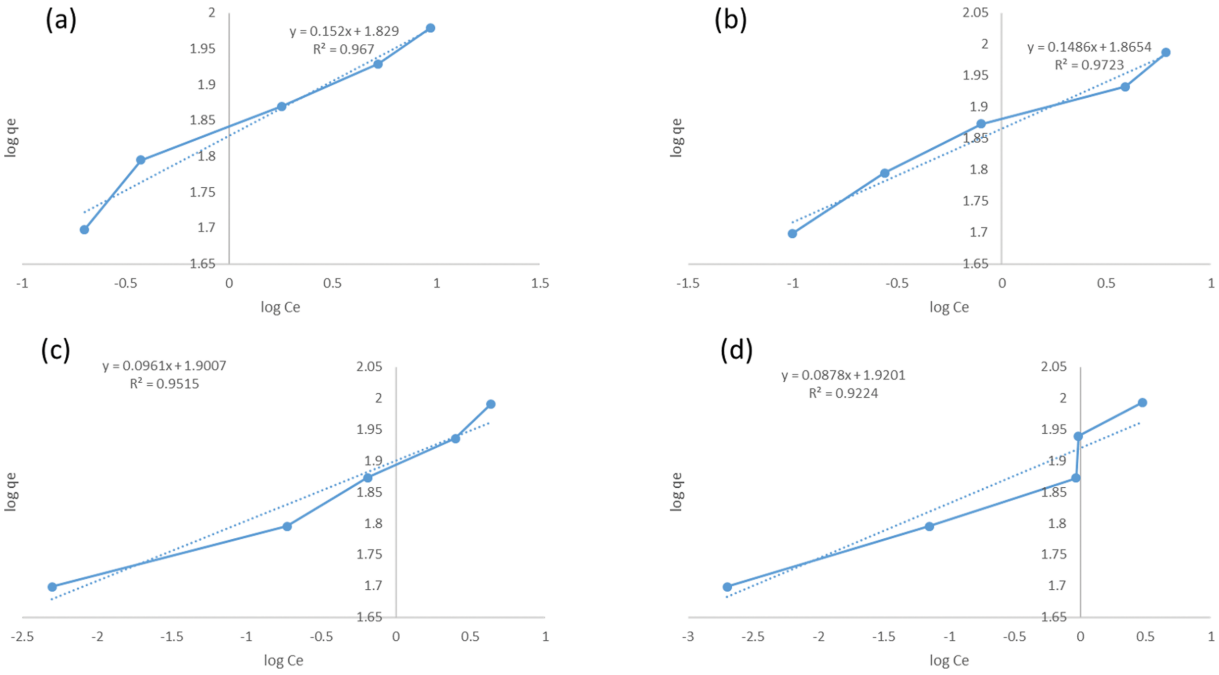


Fig. S4. Freundlich isotherm model at (a) 25 °C (b) 30 °C (c) 35 °C and (d) 40 °C.